Collective intracellular cargo transport by multiple kinesins on multiple microtubules

Kejie Chen
Department of Mechanical Engineering, University of Michigan, Ann Arbor, Michigan 48105, USA

Woochul Nam
School of Mechanical Engineering, Chung-Ang University, 84 Heukseok-ro, Dongjak-gu, Seoul 06974, Republic of Korea

Bogdan I. Epureanu*
Department of Mechanical Engineering, University of Michigan, Ann Arbor, Michigan 48105, USA

(Received 31 July 2019; revised manuscript received 6 April 2020; accepted 28 April 2020; published 28 May 2020)

The transport of intracellular organelles is accomplished by groups of molecular motors, such as kinesin, myosin, and dynein. Previous studies have demonstrated that the cooperation between kinesins on a track is beneficial for long transport. However, within crowded three-dimensional (3D) cytoskeletal networks, surplus motors could impair transport and lead to traffic jams of cargos. Comprehensive understanding of the effects of the interactions among molecular motors, cargo, and tracks on the 3D cargo transport dynamics is still lack. In this work, a 3D stochastic multiphysics model is introduced to study the synergistic and antagonistic motions of kinesin motors walking on multiple mircotubules (MTs). Based on the model, we show that kinesins attaching to a common cargo can interact mechanically through the transient forces in their cargo linkers. Under different environmental conditions, such as different MT topologies and kinesin concentrations, the transient forces in the kinesins, the stepping frequency and the binding and unbinding probabilities of kinesins are changed substantially. Therefore, the macroscopic transport properties, specifically the stall force of the cargo, the transport direction at track intersections, and the mean-square displacement (MSD) of the cargo along the MT bundles vary over the environmental conditions. In general, conditions that improve the synergistic motion of kinesins increase the stall force of the cargo and the capability of maintaining the transport. In contrast, the antagonistic motion of kinesins temporarily traps the cargo and slows down the transport. Furthermore, this study predicts an optimal number of kinesins for the cargo transport at MT intersections and along MT bundles.

DOI: 10.1103/PhysRevE.101.052413

I. INTRODUCTION

Many cellular processes, such as mitosis, the transport of proteins and organelles, and the beating of cilia and flagella, are driven by molecular motors [1,2]. Although an individual motor protein can produce continuous motion [3–5], most intracellular processes require multiple motors to function in a cooperative manner [6,7]. Since the late 2000s, the cooperative cargo transport by multiple motors along a single track, such as a microtubule (MT) or a filament, has been well characterized through experiments and mathematical models [8–13]. These studies suggest that the cooperative dynamics of motors along a track improves the reliability and efficiency of the transport because multiple motors generate large pulling forces on the cargo and help it overcome the intracellular obstacles such as MT associate proteins in the highly viscous cytoplasm [14–16].

However, several experiments observed sluggish cargo motions when multiple motors transport a cargo on intersecting tracks. Schroeder *et al.* [17] showed that cargoes transported by myosin V and dynein-dynactin are likely to be trapped at the intersection of two filaments. Ross *et al.* [18] observed the trapping of cargoes at the MT intersection by multiple kinesins. During the temporary trapping intervals, Gao *et al.* [19] showed that the intracellular cargo exhibits rapid and directional rotation driven by molecular motors. On bundles of multiple MTs, Stepanek *et al.* [20] observed the existence of distinct anterograde and retrograde transport modes. When a faster transport caught up with a slower one moving in the same direction, they would progress together at the same speed.

In addition, the concentration of motors influences the transport dynamics. Neri *et al.* [21] showed that when the motion of the cargo is dominated by a large number of kinesins, the heterogeneity of cargo distribution depends on the complexity of the entire track network. When few motors are involved in the transport and the cargo can easily unbind from the track, the cargo distribution is influenced only by the local track topology. Shubeita *et al.* [22] found that the average transport velocity of the lipid droplets in the embryos is around 5.5% higher when the concentration of the kinesin is reduced. Other studies observed traffic jams of cargoes along MTs when the motor density exceeds a critical value [23–25]. These observations suggest that the transport speed and distance of the cargo may not necessarily be improved by a large number of motors in dense MT networks. Considering that the force generated by a single motor is not sufficient

*Corresponding author: epureanu@umich.edu

to overcome the load fluctuations on a cargo, an optimal concentration of motors could exist for achieving fast and robust transport on multiple MTs.

To elucidate the complex transport dynamics, this work proposed a three-dimensional (3D) stochastic dynamical model to study the collective behavior of multiple kinesins on multiple MTs. The model captures transient multiphysical phenomena during the transport, including walking, binding, and unbinding of kinesins; diffusion of the cargo; and interactions between kinesins, cargo, and MTs. The model predictions are verified based on the distribution of the stall force along a MT and the transport dynamics at a 90° intersection of two MTs measured in previous experiments [18]. The stall force is affected by the nonuniform distribution of external loads among all bound kinesins (explicitly, kinesins that bind and walk on a MT). The transport direction at a 90° intersection of two MTs is likely to be switched when one MT disrupts cargo diffusion and the free kinesins bind to the intersecting track. Next, the collective transport of the cargo by different number of kinesins in different MT topologies was studied. Fixing the number of kinesins on the cargo, two perpendicularly intersecting MTs with intermediate separating distance are shown to have the largest influence on the transport. Inside the same topology of MTs, an intermediate number of kinesins achieves the largest switching and passing probabilities at the 90° MT intersection, and the fast cargo mobility (characterized by the mean-square displacement) along the MT bundle. Analysis of the microscopic dynamics of kinesins further helps to illustrate that the impairment of the transport at a large number of kinesins comes from the antagonistic motion of the kinesins that are lagged behind the center of the cargo. Moreover, the transport along a MT bundle interrupted by a neighboring MT was investigated. Overall, the three-dimensional (3D) dynamical model and the predictions suggest that the intracellular transport can be adjusted by controlling MT topologies and the number of kinesins.

II. MODEL

Consider the case where N identical kinesins are uniformly distributed on the surface of a spherical cargo. The connection between cargo and kinesins are assumed to be intact. Kinesins (K) can bind to and unbind from the MTs. When a kinesin binds to and walks on the MT, it exerts force and moment to the cargo. Thus, kinesins interact mechanically and cargo undergoes Brownian motion influenced by the total force and moment generated by bound kinesins.

To study the collective dynamics of multiple kinesins, most previous modeling works focus on the 1D motion along the axial direction of a single MT. Assuming the velocity, binding and unbinding rates are constants, the probability of having n bound motors at time t was described by a continuous time Markov process [15,26–28]. Several studies further considers the fact that a motor cannot bind to positions occupied by other motors. Therefore, the distribution of motors on the MT is described by the totally asymmetric simple exclusion process [23–25,29]. However, since the properties of the kinesin are influenced by the force it experiences [30,31] and the force fluctuates due to the cargo diffusion and the interactions between kinesins and MTs, Monte Carlo–based computational models were proposed to include the force-dependent stepping rates and unbinding rates of kinesins [12,32–34]. For example, the stepping motion of a kinesin can be modeled as a Poisson process with a rate exponentially decaying with the force [32]. The force-dependent unbinding rate are modeled based on the Bell model [35]. Combining the Monte Carlo model with the experiments, it was shown that the transport by pairs of kinesin-1 and kinesin-3 is dominated by the motion of kinesin-1 because kinesin-1 walks slower and has a smaller unbinding probability than kinesin-3 [32]. Blackwell *et al.* [36] considers the forward and backward stepping motion of motors and modeled the stepping rate through an energy perspective. They found that the Brownian ratchetlike dynamics of motor stepping (specifically, the asymmetric forward and backward stepping rates) lead to fast cargo transport. Recently, Bergman *et al.* [37] developed a 3D dynamical model to study the effects of a MT intersection on the transport and predict the transport directions.

In this work, there are three major improvements compared to previous models. (1) The MTs are modeled as cylinders with discrete binding sites distributed on the surface of the MT. The 3D stepping motion of kinesins influenced by the force along the axial and tangential direction of the MT is considered. (2) The geometrical constraint of the MTs on kinesin binding and cargo diffusion is considered. (3) Kinesin stepping motion is described by the mechanochemical cycle on its heads. The influence of the force on the chemical reaction speed and the unbinding probability are modeled separately at different chemical reaction states. Specifically, the model considers that the most susceptible state to the force is when the ATP releases from the MT bound head, as suggested by previous experimental findings [38]. In addition, the influence of ATP concentration on the kinesin dynamics is included. Note that the dynamics described by the model is no longer a Markov process. The transition between the states of the system is determined by the microscopic interactions among kinesins, cargo, and MTs. Thus, the transition is spatial-temporal dependent as well as history dependent.

In the model, the dynamics of a kinesin i is characterized by six time-dependent variables, $\boldsymbol{X}_{hi}(t)$, $\boldsymbol{X}_{ki}(t)$, $P_{Ki}(t)$, $P_{\mathrm{ATP},i}(t)$, $P_{bi}(t)$, and $P_{ubi}(t)$. $\boldsymbol{X}_{hi}(t)$ is a vector containing the position of the center of the two kinesin heads at time t. $\boldsymbol{X}_{ki}(t)$ is a vector containing the position where kinesin i attaches on the cargo surface. P_{Ki} and $P_{\mathrm{ATP},i}$ are the probabilities of staying at chemical reaction states [K + ATP] and [K.ATP]. $P_{bi}(t)$ is the binding probability. $P_{ubi}(t)$ is the unbinding probability. The Monte Carlo simulation described in Algorithm 1 is used to calculate the evolution of the system under predefined environmental conditions. Initially, the cargo is located at a position near the MTs, and all kinesins are unbound from the track. A time step Δt is chosen as 0.001 s for simulations. At each time step, five parts of the system are updated: (1) The translational and rotational motions of the cargo, characterized by $(\boldsymbol{X}_{\mathrm{cg}}, \boldsymbol{\theta}_{\mathrm{cg}})$, are updated based on the diffusion motion. $\boldsymbol{X}_{\mathrm{cg}}$ is a vector containing the position of cargo center. $\boldsymbol{\theta}_{\mathrm{cg}} = [\theta_x, \theta_y, \theta_z]$ is a vector containing the angular position of the cargo center, where θ_x, θ_y, and θ_z are angles with respect to the x, y, and z axes. (2) Force $\boldsymbol{F}_i$ and moment $\boldsymbol{M}_i$ exerted on the cargo are calculated. (3) For each bound kinesin i, the chemical reaction, represented by the two probabilities P_{Ki}

Algorithm 1. The stochastic dynamic model. r_{1i}, r_{2i}, r_{bi}, r_{ubi} are independent and identically distributed random variables. Function Walk () updates the chemical reaction states and the positions of kinesin heads, discussed in Sec. II A. Function Diffuse () updates the cargo position, discussed in Sec. II B. Function Force () calculates the force and moment exerted by a kinesin, discussed in Sec. II C. Function Bind () and function Unbind () calculate the probabilities for a kinesin to bind to or unbind from a MT, discussed in Secs. II D and II E.

Input: For all kinesins $i = 1, 2, \ldots, N$:
$(P_{Ki},\ P_{\mathrm{ATP},i},\ P_{bi},\ P_{ubi},\ t_{bi},\ t_{ubi},\ state\_i,\ onMT\_i) \longleftarrow (1,\ 0,\ 0,\ 1,\ 0,\ 0,\ 1,\ 0)$
$(\boldsymbol{F}_i,\ \boldsymbol{M}_i) \longleftarrow (\boldsymbol{0},\ \boldsymbol{0})$
$(r_{1i},\ r_{2i},\ r_{bi},\ r_{ubi}) \longleftarrow$ independent and identically distributed Uniform(0, 1)
For cargo: $(\boldsymbol{\theta}_{\mathrm{cg}},\ \boldsymbol{X}_{\mathrm{cg}})$
for $t = 1$ **to** N_t **do**
  $(\boldsymbol{\theta}_{\mathrm{cg}}, \boldsymbol{X}_{\mathrm{cg}}) \longleftarrow$ Diffuse$(\boldsymbol{\theta}_{\mathrm{cg}}, \boldsymbol{X}_{\mathrm{cg}}, \boldsymbol{F}_1, \boldsymbol{F}_2, \ldots, \boldsymbol{F}_N, \boldsymbol{M}_1, \boldsymbol{M}_2, \ldots, \boldsymbol{M}_N)$
  for $i = 1$ **to** N **do**
    if $onMT\_i > 0$ **then**
      $t_{ubi} \longleftarrow t_{ubi} + 1$
      $(\boldsymbol{F}_i,\ \boldsymbol{M}_i) \longleftarrow$ Force$(\boldsymbol{X}_{hi}, \boldsymbol{\theta}_{ki}, \boldsymbol{X}_{\mathrm{cg}}, \boldsymbol{\theta}_{\mathrm{cg}})$
      $(P_{Ki}, P_{\mathrm{ATP},i}, \boldsymbol{X}_{hi}, r_{1i}, r_{2i}, state\_i) \longleftarrow$ Walk$(P_{Ki}, P_{\mathrm{ATP},i}, \boldsymbol{X}_{hi}, \boldsymbol{F}_i, r_{1i}, r_{2i}, state_i)$
      $(\boldsymbol{F}_i,\ \boldsymbol{M}_i) \longleftarrow$ Force$(\boldsymbol{X}_{hi}, \boldsymbol{\theta}_{ci}, \boldsymbol{X}_{\mathrm{cg}}, \boldsymbol{\theta}_{\mathrm{cg}})$
      $P_{ubi} \longleftarrow$ Unbind$(\boldsymbol{F}_i,\ \boldsymbol{M}_i, t_{ubi}, state_i)$
      if $P_{ubi} \geqslant r_{ubi}$ **then**
        $(P_{Ki},\ P_{\mathrm{ATP},i},\ P_{ubi},\ \boldsymbol{F}_i,\ \boldsymbol{M}_i,\ t_{ubi}, onMT\_i) \longleftarrow (1,\ 0,\ 0,\ \boldsymbol{0},\ \boldsymbol{0},\ 0,\ 0)$
        $r_{ubi} \longleftarrow Uniform(0, 1)$
       end if
      end if
      if $onMT\_i = 0$ **then**
        $t_{bi} \longleftarrow t_{bi} + 1$
        $(\boldsymbol{X}_{hi},\ P_{bi}) \longleftarrow$ Bind$(\boldsymbol{X}_{\mathrm{cg}},\ \boldsymbol{\theta}_{\mathrm{cg}},\ \boldsymbol{\theta}_{ki},\ t_{bi})$
        if $P_{bi} \geqslant r_{bi}$ **then**
          $(P_{bi},\ t_{bi},\ onMT\_i) \longleftarrow (0,\ 0,\ 1)$
          $(r_{1i},\ r_{2i},\ r_{bi}) \longleftarrow$ independent and identically distributed Uniform(0, 1)
        end if
      end if
    enf for
  enf for
Output: $(\boldsymbol{\theta}_{\mathrm{cg}},\ \boldsymbol{X}_{\mathrm{cg}},\ \boldsymbol{X}_{hi},\ \boldsymbol{F}_i)_t$, for $i = 1, 2, \ldots, N$ and $t = 1, 2, \ldots, N_t$.

and $P_{\mathrm{ATP},i}$, as well as the center position of two kinesin heads $\boldsymbol{X}_{hi}$ are updated. When the number of bound kinesins on the MT is n, the calculation of P_{Ki}, $P_{\mathrm{ATP},i}$, and $\boldsymbol{X}_{hi}$ are performed n times at every time step. (4) For each bound kinesin i, the unbinding probability P_{ubi} are calculated. The calculation of unbinding probabilities is performed n times at every time step. (5) For each unbound kinesin j, the binding probability P_{bj} are calculated. When there are N kinesins on the cargo and n of them bind to the MT, the calculation is performed $N - n$ times at each time step. It should be noted that the six book-keeping variables, $\boldsymbol{X}_{hi}(t)$, $\boldsymbol{X}_{ki}(t)$, $P_{Ki}(t)$, $P_{\mathrm{ATP},i}(t)$, $P_{bi}(t)$, and $P_{ubi}(t)$, are updated simultaneously at every time step. However, the kinesin dynamics including the transitions between chemical reaction state, unbinding and rebinding are characterized by $P_{Ki} \leqslant r_{1i}$, $P_{\mathrm{ATP},i} + P_{Ki} \leqslant r_{2i}$, $P_{ubi} \geqslant r_{ubi}$, and $P_{bi} \geqslant r_{bi}$, respectively. These kinesin dynamics occur in a sequential manner in the model.

A. The walking motion of kinesin

Kinesins, powered by adenosine triphosphate (ATP), walk in a stepwise fashion on a MT [5,39,40]. The kinesin motor composes of a long cargo linker, two short neck linkers and two heads, as shown in Fig. 1(d). During the kinesin walking motion, each kinesin head occupies one tubulin binding site on the MT. An ATP binds to the leading kinesin head, causing a conformational change in the molecule. The trailing kinesin head diffuses to the next binding site. Three discrete

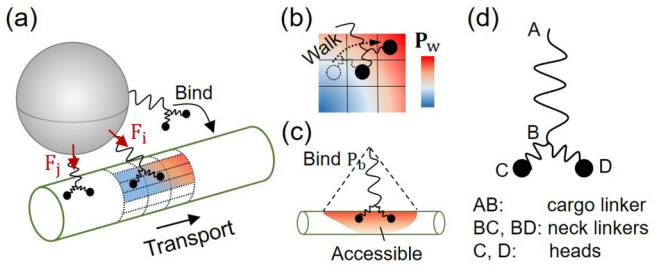

FIG. 1. Schematic illustration of the stochastic dynamic model. (a) A cargo is transported by two kinesins along a MT. The MT consists of 13 protofilaments in the tubular arrangement. (b) In each step, the trailing kinesin head diffuses to one of the binding sites surrounding the leading head. The probability for the trailing head to bind to one of the neighboring sites is represented by a probability vector $\boldsymbol{P}_w$. (c) As cargo diffuses around, other unbound kinesins could reach the MT and bind to it. The binding probability P_b is influenced by the area on the MT surfaces that is reachable to the unbound kinesin heads. (d) The simplified structure of the kinesin consists of two heads, two neck linkers, and a cargo linker.

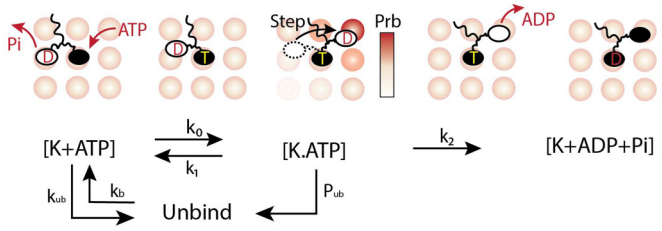

FIG. 2. The mechanochemical cycle and the stepping motion of the kinesin.

chemical states, [K + ATP], [K.ATP], and [K + ADP+Pi], are used to describe the mechanochemical cycle on kinesin heads (Fig. 2), where K represents kinesin, ADP represents Adenosine diphosphate, and Pi represents phosphate. At state [K+ATP], the leading head is in the nucleotide free state and strongly bind to the MT while another head is loosely attached to the MT. Then, an ATP binds to the leading head and causes a conformational change in the kinesin molecule. At state [K.ATP], the trailing head diffuses to the next binding site and the stress caused by the conformational change is released. By dissociating ADP, the free head strongly binds to the next binding site. At state [K + ADP+Pi], the ATP on the leading head is hydrolyzed into ADP and phosphate. The probabilities of kinesin i to be at states [K + ATP], [K.ATP], and [K + ADP+Pi] are denoted as P_{Ki}, $P_{\mathrm{ATP},i}$, and $P_{\mathrm{ADP},i}$, respectively. These probabilities are calculated as

$$\frac{d}{dt}P_{Ki} = -k_0\, c_{\mathrm{ATP}} P_{Ki} + k_2 P_{\mathrm{ATP},i}, \tag{1}$$

$$\frac{d}{dt}P_{\mathrm{ATP},i} = k_0\, c_{\mathrm{ATP}} P_{Ki} - k_1 P_{\mathrm{ATP},i} - k_2 P_{\mathrm{ADP},i}, \tag{2}$$

$$\frac{d}{dt}P_{\mathrm{ADP},i} = k_2 P_{\mathrm{ATP},i}, \tag{3}$$

$$P_{Ki} + P_{\mathrm{ATP},i} + P_{\mathrm{ADP},i} = 1. \tag{4}$$

where c_{ATP} is the concentration of ATP ($c_{\mathrm{ATP}} = 1250\ \mu$M in this work). Transition rates k_0 and k_2 are assumed to be constants. k_1 is influenced by the magnitude of the force $\boldsymbol{F}_i$ in kinesin i, because the most susceptible state to the external load is when the ATP releases from the MT bound head [38]. k_1 is calculated based on the equation suggested by Hendricks *et al.* [41] as

$$k_1 = k_{10}\, \exp\left[\frac{k_{11}\left(\frac{|\boldsymbol{F}|}{k_{11}} - k_{12}\right)^2}{2k_B\, T}\right]. \tag{5}$$

Parameters k_0, k_{10}, k_{11}, k_{12}, and k_2 are obtained based on experimentally observed force-velocity curves over various ATP concentrations [42,43].

At state [K.ATP], the short neck linkers of the two kinesin heads constrain the reachable binding sites of the trailing head. The force inside the kinesin influences the probabilities of the trailing head to bind to a specific site. In previous models, the MT is regarded as a 1D line, so kinesin only takes steps forward or backward [37,44]. In 3D, however, a kinesin can step along both the longitudinal and tangential directions of the MT. Therefore, the processivity of the kinesin, which is defined as the velocity of kinesin moving along the longitudinal direction of the MT, is influenced by two factors, the stepping rate and the probability of the trailing head to bind to a forward binding site along the longitudinal direction. In particular, a coarse-grained mechanical model proposed in previous study [45] is used to calculate the stepping probability $\boldsymbol{P}_w$ under an external force $\boldsymbol{F}$. The results of $\boldsymbol{P}_w(\boldsymbol{F})$ are provided in in the Supplemental Material at [46].

B. Cargo diffusion

Function Diffuse () calculates the transnational and rotational position of cargo center ($\boldsymbol{X}_{\mathrm{cg}}$ and $\boldsymbol{\theta}_{\mathrm{cg}}$) as

$$\frac{d}{dt}\boldsymbol{\theta}_{\mathrm{cg}} = \frac{\sum_{i=1}^{n}\boldsymbol{M}_i}{8\pi\, R^3\, \delta} + \boldsymbol{r}(\sqrt{2D_r}), \tag{6}$$

$$\frac{d}{dt}\boldsymbol{X}_{\mathrm{cg}} = \frac{\sum_{i=1}^{n}\boldsymbol{F}_i}{6\pi\, R\, \delta} + \boldsymbol{r}(\sqrt{2D_t}). \tag{7}$$

where R is the cargo radius, $\sum_{i=1}^{n}\boldsymbol{F}_i$ and $\sum_{i=1}^{n}\boldsymbol{M}_i$ are the total force and moment exerted on the cargo by n bound kinesins, $\delta = 8.9 \times 10^{-4}$ Pa s is the fluid viscosity of water. $D_t = \frac{k_B T}{6\pi R\delta}$ and $D_r = \frac{k_B T}{8\pi R^3 \delta}$ are the transnational and rotational diffusion coefficients, respectively. $\mathbf{r}(\sigma)$ is a vector composed of normally distributed random numbers with standard deviation σ and zero average. The torque $\boldsymbol{M}_i$ is calculated as $\boldsymbol{M}_i = (\boldsymbol{X}_{ki} - \boldsymbol{X}_{\mathrm{cg}}) \times \boldsymbol{F}_i$, where $\boldsymbol{X}_{ki}$ represents the binding position between kinesin i and the surface of the cargo. $\boldsymbol{X}_{\mathrm{cg}}$ is the position of cargo center. Note that the thermal diffusion of the cargo is much faster than the walking motion of kinesins. Thus, in the function Diffuse (), the time step used to calculate the cargo diffusion is 0.0001 s.

C. Force inside the kinesin

The effective length of the kinesin motor is approximated by the distance between the center of the two heads and the end of the cargo linker as $|\boldsymbol{X}_{ki} - \boldsymbol{X}_{hi}|$. The force inside the kinesin i caused by the extension of the kinesin motor is calculated as

$$\boldsymbol{F}_i = \frac{\boldsymbol{X}_{ki} - \boldsymbol{X}_{hi}}{|\boldsymbol{X}_{ki} - \boldsymbol{X}_{hi}|}\,(|\boldsymbol{X}_{ki} - \boldsymbol{X}_{hi}| - L_k)S_k, \tag{8}$$

where L_k is the unstretched length of the kinesin motor, and S_k is the stiffness of the cargo linker. Note that, a cablelike linker is used in the model, because it was observed in previous experiments [47] that the stiffness of kinesin is an order of magnitude lower for compression than for stretching. Thus, $\boldsymbol{F}_i = \boldsymbol{0}$ when $|\boldsymbol{X}_{ki} - \boldsymbol{X}_{hi}| \leqslant L_k$. Moreover, in our model and many other studies [32,37], the contour length of the kinesin molecule is used for L_k. However, experimental results [48] show that active kinesin molecules function in a compact configuration and their effective length is only around 17 nm. A shorter cargo linker length would reduce the number of kinesins that bind to the MTs and affect the transport dynamics. For example, in an environment crowded with MTs, with a shorter cargo linker length, less kinesins can bind to the nearby MTs. The trapping of the cargo by the antagonistic motions of kinesins on different MTs can be diminished. $\boldsymbol{X}_{ki}$, the binding position of kinesin i on the cargo surface, is calculated as

$$\boldsymbol{X}_{ki} = \boldsymbol{X}_{\mathrm{cg}} + R\,[\sin\beta_i\cos\alpha_i,\ \sin\beta_i\sin\alpha_i,\ \cos\beta_i], \tag{9}$$

Algorithm 2. The kinesin walking modular. state_$i = 1$ represents [K+ATP] state; state_$i = 2$ represents [K.ATP] state; and state_$i = 3$ represents [K+ADP+Pi] state. The chemical reaction always starts from [K+ATP] state. Thus, when a kinesin starts to bind to and walk along the MT, P_{Ki} is set to 1. P_{Ki} decreases over time and when P_{Ki} becomes smaller than the random number r_{1i}, the chemical state changes to [K.ATP]. The time duration at [K.ATP] state measured in the experiments is much shorter than the time duration at the other two states [9,31]. Thus, after the kinesin takes a step forward at state [K.ATP], the chemical state changes to [K+ADP+Pi] immediately.

Input: P_{Ki}, $P_{\mathrm{ATP},i}$, $\boldsymbol{X}_{hi}$, $\boldsymbol{F}_i$, t_{ubi}, r_{1i}, r_{2i}, $state\_i$
  if $state\_i = 1$ **then**
    Update P_{Ki} and $P_{\mathrm{ATP},i}$ based on Eqs. (2)–(4)
    if $P_{Ki} \leqslant r_{1i}$ **then**
      $state\_i \longleftarrow 2$
    end if
  else if $state\_i = 2$ **then**
    Update $\boldsymbol{X}_{hi}$ based on $\boldsymbol{P}_w(\boldsymbol{F}_i)$
    $state\_i \longleftarrow 3$
  else
    Update P_{Ki} and $P_{\mathrm{ATP},i}$ based on Eqs. (2)–(4)
    if $P_{\mathrm{ATP},i} + P_{Ki} \leqslant r_{2i}$ **then**
      $(P_{Ki}, P_{\mathrm{ATP},i}, t_{ubi}, state\_i) \longleftarrow (1, 0, 0, 1)$
      $(r_{1i}, r_{2i}) \longleftarrow$ independent and identically distributed Uniform (0, 1)
    end if
  end if
Output: P_{Ki}, $P_{\mathrm{ATP},i}$, $\boldsymbol{X}_{hi}$, r_{1i}, r_{2i}, $state\_i$

where α_i and β_i are azimuthal angle and polar angle shown in Fig. 3.

D. Binding of kinesin

The binding of kinesins to a single MT is usually described by a Poisson process with a constant rebinding rate k_b [37],

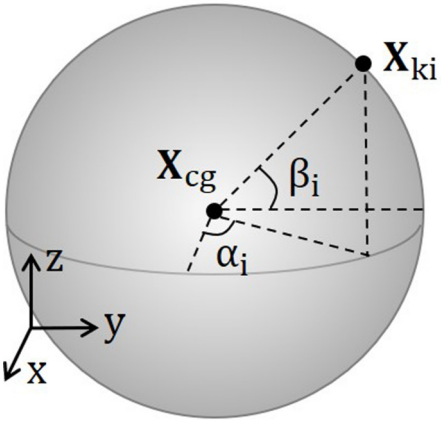

FIG. 3. Schematic illustration of the binding position between a kinesin and a cargo. The binding position between kinesin i and the surface of the cargo is $\boldsymbol{X}_{ki}$. The cargo center is $\boldsymbol{X}_{\mathrm{cg}}$. Because kinesins are uniformly distributed on the surface of the cargo, the characteristic angles are calculated as $\alpha_i = 2\pi u$ and $\beta_i = \cos^{-1}(2v - 1)$, where u and v are random numbers uniformly distributed between 0 and 1.

TABLE I. Parameters of the model. The third column is the reference of the experimental data used to acquire the corresponding parameter. The parameters of each kinesin i are identical and have values shown in Table I. Specifically, the parameters for chemical reaction rates and unbinding rates are acquired in our previous work [50]. The rebinding rate is acquired in the work [49].

Unstretched length, L_k	60 nm	Kerssemakers *et al.* [48]
Stiffness, S_k	0.3 pN/nm	Jeney *et al.* [47,51]
Chemical reaction, k_0	0.0283 $\mu\mathrm{M}^{-1}\mathrm{S}^{-1}$	Schnitzer *et al.* [42]
Chemical reaction, k_2	98.875 s^{-1}	Schnitzer *et al.* [42]
Chemical reaction, k_{10}	32.921 s^{-1}	Schnitzer *et al.* [42]
Chemical reaction, k_{11}	3.302 pN/nm	Schnitzer *et al.* [42]
Chemical reaction, k_{12}	1.2114 nm	Schnitzer *et al.* [42]
Unbinding, k_{u0}	2.65×10^{-6} s^{-1}	Schnitzer *et al.* [42]
Unbinding, P_{u0}	0.01	Schnitzer *et al.* [42]
Unbinding, d_0	0.0054 nm	Schnitzer *et al.* [42]
Unbinding, d_1	1.064 nm	Schnitzer *et al.* [42]
Rebinding, k_{b0}	1.3×10^{4} s^{-1}	Ross *et al.* [18]

which was measured in experiments to be 5 s^{-1} [13]. At the MT intersection, the binding rate is influenced by the relative positions of kinesins and MTs. Thus, the probability of a free kinesin i bind to the MTs is calculated as

$$P_{bi}(t_b) = 1 - e^{-k_b t_b}, \tag{10}$$

$$k_b = k_{b0}\frac{V_b}{V_d}, \tag{11}$$

where k_b is the rebinding rate. V_b is the volume surrounding the MT where the kinesin heads can bind; V_d is the volume where the kinesin heads can diffuse. V_b and V_d are calculated based on the fast marching method, as described in previous work [49]. The values of V_b and V_d near a single MT and at a 90° MT intersection are provided as Supplemental Material at [46]. k_{b0} is a model parameter (Table I). Note that the probability $P_{bi}(t_b)$ is calculated only for nonengaged kinesins. t_b represents the time interval from the kinesin unbinding moment to current time.

E. Unbinding of kinesin

The force-dependent unbinding probability of kineins i is calculated based on the Bell formula in several recent studies [15,16,32,37,44]. Bell first showed that the unbinding rate between a ligand and its receptor is influenced by the force applied to pull the complex apart [35]. The unbinding rate follows the expression $k_{ub} = k_{u0}\exp(\frac{fd}{k_BT})$, where k_{u0} is the unbinding rate without force, f is the magnitude of the force, and d is the changes of the distance of the ligand and receptor from the bound state to the transition state [38]. Berger *et al.* [52] derived analytical expressions for the probability distribution of the unbinding force, and estimated the force-dependent unbinding rate based on the force traces data, without prior information of force velocity relations. In our model, the unbinding probability is calculated at states [K + ATP] and [K.ATP]. At state [K + ADP+Pi], the unbinding probability is negligible because both kinesin heads strongly bind to the MT. The average time the kinesin spends at [K + ATP] state is

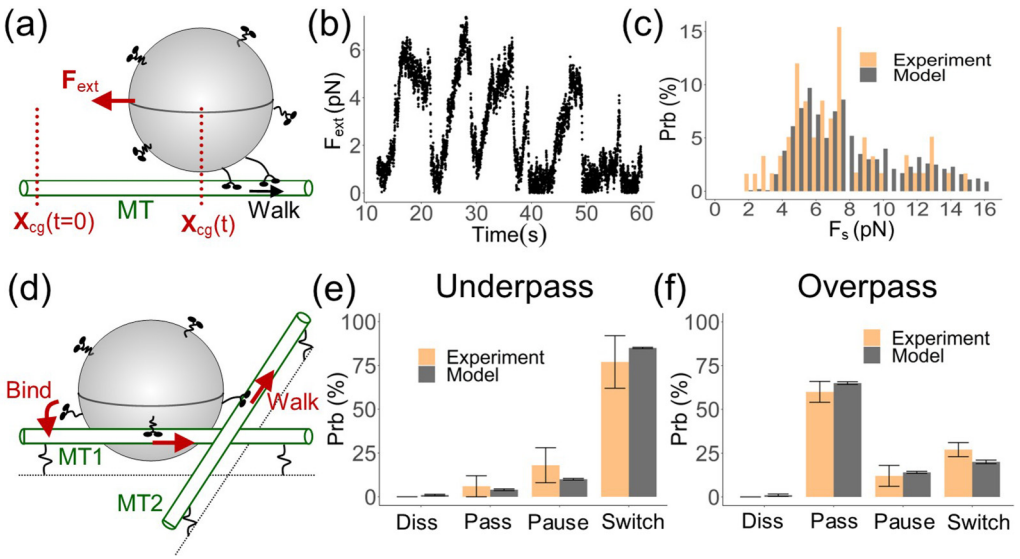

FIG. 4. Verification of the stochastic multiphysics model. (a) To calculated the stall force, the cargo is transported by kinesins on a single MT under an external load $\boldsymbol{F}_{\text{ext}}$. (b) The variation of the force F_{ext} applied by kinesins on the cargo along the MT direction. (c) The distribution of the stall force F_s. (d) Schematic illustration of the transport dynamics at a 90° MT intersection. (e) Probabilities for the cargo to pass, pause, switch or dissociate at the intersection when it is moved on the bottom MT (MT1) to the intersection (i.e., underpass). (f) Probabilities of the cargo dynamics when it is transported on the top MT (MT2) to the intersection (i.e., overpass). The experimental data are from the previous study [18].

at millisecond level, while the average time for state [K.ATP] is at microsecond level [9,31]. Although the duration of state [K.ATP] is short, the unbinding probability at [K.ATP] is not negligible, because at this state the affinity between kinesin and MT is the weakest among the whole mechanochemical cycle [53]. Thus, the unbinding at state [K.ATP] is modeled as an unbinding probability P_{ubi} as

$$P_{ubi} = P_{u0} \exp\left[\frac{|\boldsymbol{F}_i|d_0}{k_BT}\right], \tag{12}$$

The unbinding at state [K + ATP] is described based on an unbinding rate k_{ub} (i.e., unbinding probability per unit time). The unbinding probability P_{ubi} is calculated as

$$P_{ubi}(t_u) = 1 - e^{-k_{ub}t_u}, \tag{13}$$

$$k_{ub} = k_{u0} \exp\left[\frac{|\boldsymbol{F}_i|d_1}{k_BT}\right], \tag{14}$$

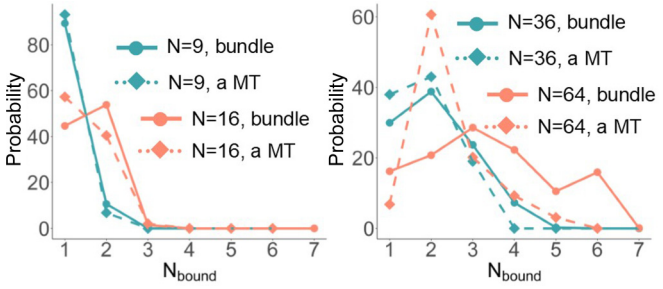

FIG. 5. The distribution of the number of kinesins that bind to a single MT or a bundle of two parallel MTs N_{bound} over the different number of kinesins on the cargo N.

Parameters for the unbinding model, P_{u0}, d_0, k_{u0}, d_1, are acquired by fitting the model to the force-dependent run lengths [42] (Table I). t_u is the total time since the kinesin binds to the MT. Note that the unbinding rate k_{ub} changes over time. Thus, a more accurate formula for the unbinding probability is $P_{ub}(t_u) = 1 - \exp[\int_0^{t_u} k_{ub}(s)ds]$.

The model proposed in Ref. [37] also predicts the 3D motion of the cargo when it is transported by multiple kinesins. The model presented herein considers additional features to enrich fidelity. First, kinesin can take sideway, backward, and forward steps on a MT. The sideway and backward walking motions have been observed by several previous studies [54]. The stepping direction of a kinesin is affected by other nearby molecules, such as other kinesins or other molecules bound on the MT. In addition, when two MTs are very close, they mechanically block parts of the binding sites on each other. Second, the cargo motion and kinesins head diffusion affect the binding probability. When there are more binding sites that kinesin heads can reach, the binding probability is increased. As a result, the binding probability fluctuates with the distance between the cargo and the MTs. A kinesin connecting the cargo to a MT brings the cargo close to that MT, and that enhances the probability of other kinesins on the cargo to bind to the same MT. Third, a comprehensive model of the chemical reaction cycle on kinesin heads allows predictions of the effect of ATP concentration on the collective kinesin dynamics.

III. RESULTS

A. Model verification

The 3D dynamical model is verified based on previous experimental studies [18] of kinesins transporting polystyrene cargoes at a 90° intersection of two MTs [18]. In the

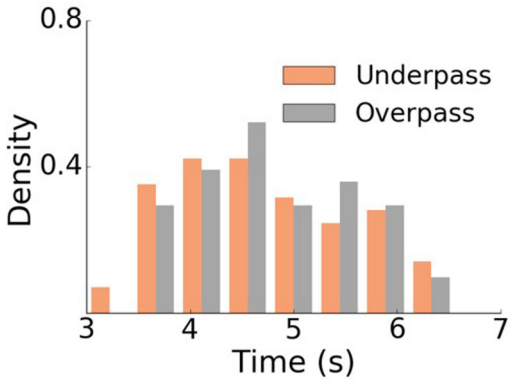

FIG. 6. The distribution of the dwell time T_d at the intersection. T_d is calculated as $T_d = T_e - T_b$, where T_b is the time when the cargo starts to move from a position located 1 μm away from the intersection, T_e is the time when the cargo passes the intersection and moves 1 μm away from the intersection.

experiments, first, 800-nm polystyrene cargoes were incubated with various concentrations of kinesins to allow different numbers of kinesins to attach to the surface of the cargo. After the binding between kinesins and cargoes reaches equilibrium, the medium was removed. Next, an optical trap was used to place the cargo near a single MT or an intersection of two MTs. The stall forces of the cargoes incubated with two different kinesin concentrations were measured using the optical trap. When the concentration of kinesin is 0.001 μg/ml, it is estimated that only one kinesin is attached to a cargo. The measured stall force distribution follows a normal distribution with mean value of 4.2 pN. More than two kinesins are expected to be attached to the cargo when the kinesin concentration in the medium is 0.02 μg/ml. However, the exact number of kinesins was not determined in the experiment [18]. To acquire the approximate number of kinesins at a concentration of 0.02 μg/ml, the distributions of stall force of a 800 nm cargo are calculated using the model for different numbers of kinesins and compared with experimental measurements [18]. In the calculation, an external force $\boldsymbol{F}_{\text{ext}}$ parallel to the MT but opposite to the kinesin walking direction is applied to the cargo. To simulate the behavior of the cargo under the optical trap, the external force is assumed to be proportional to the moving distance of the cargo. Specifically, the magnitude of the external force is calculated as $F_{\text{cg}} = k_{\text{eff}}[X_{\text{cg}}(t) - X_{\text{cg}}(t = 0)]$, where the effective stiffness k_{eff} is 0.07 pN/nm, similar to the experimental setup [55]. X_{cg} is the cargo displacement along the MT direction [Fig. 4(a)].

Figure 4(b) shows the variation of F_{ext} calculated using the model. The external force F_{ext}, which is also equal to the total force generated by kinesins along the MT direction, increases as the cargo moves away from the starting point. When the cargo is stalled, F_{ext} stops increasing and slightly fluctuates around the maximum value. After a few seconds, all kinesins unbind from the MT and the cargo returns to the starting point. Then F_{ext} decreases to 0 pN accordingly. Afterward, cargo diffuses around the starting point until one or more kinesins bind to the MT and the active transport starts again. It is assumed the cargo is stalled when the variation of F_{ext} is less than 2 pN within 2 s. F_s is calculated as the average of F_{ext} during this 2 s time interval. When 36 kinesins are attached to the cargo surface, the stall force distribution calculated using the model shows a good agreement with the distribution measured in the experiments [18] when the kinesin concentration is 0.02 μg/ml [Fig. 4(c)].

When the cargo is placed next to a single MT and the number of kinesins N is 36, one or two kinesins are walking on the MT most of the time (Fig. 5). The stall force of one

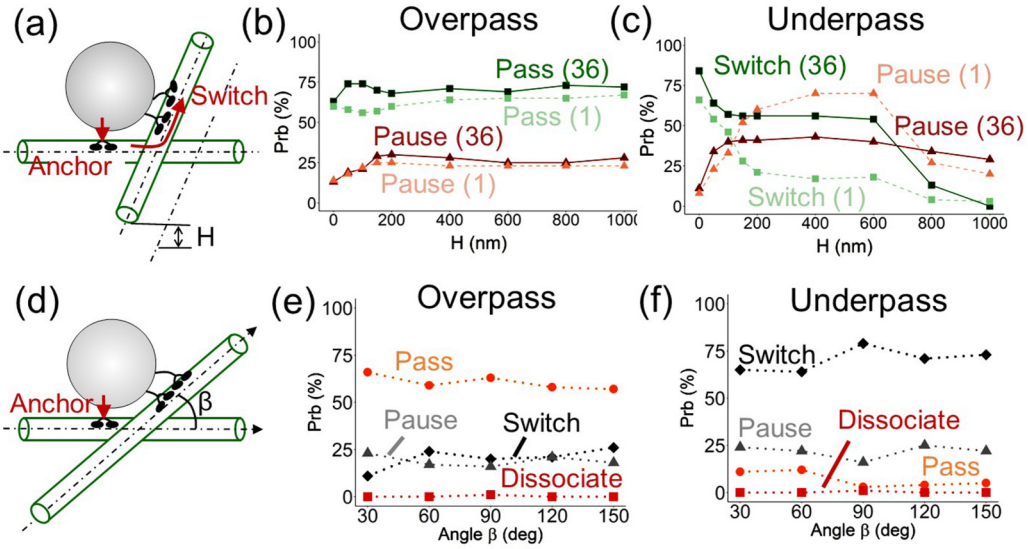

FIG. 7. Transport dynamics at the intersection of two MTs is influenced by the intersection distance H and the angle β. (a) The schematic illustration of the intersection distance H. (b) The influence of H on the passing and pausing probabilities in the overpass situation when 1 or 36 kinesins are attached on the cargo. (c) The influence of H on the switching and pausing probabilities in the underpass situation. Increasing the intersection distance significantly disrupts the transport in the underpass situation. Multiple kinesins on the cargo (36 kinesins in the case) reduces the impairment of H on the transport. (d) A schematic illustration of the intersection angle β when two MTs are attached to each other. [(e) and (f)] Transport dynamics influenced by the angle β in the overpass and underpass situations.

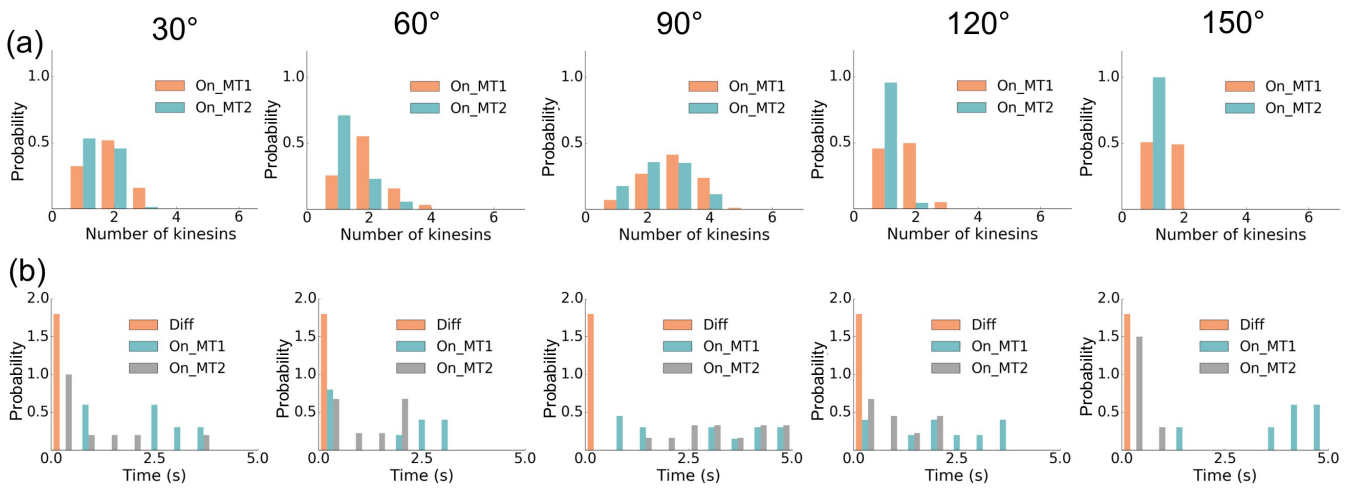

FIG. 8. The influence of intersection angle β on the transport dynamics in the underpass situation. (a) The distribution of the number of kinesins on MT1 and MT2 at the intersection when N is 36. (b) The distribution of the association time on the two MTs as well as the diffusion time. The association time on a MT is defined as the time interval when at least one kinesin binds to that MT.

engaged kinesin follows a Gaussian distribution with a mean value of 4.2 pN. The stall force of two engaged kinesins would be a Gaussian distribution of mean 8.4 pN if the load on the cargo were equally distributed among kinesins. Thus, the distribution of the stall force when $N = 36$ would have two peaks at 4.2 and 8.4 pN. However, both the experiments [18] and simulations show that the two peaks in the distribution of the stall force are not exactly 4.2 and 8.4 pN. Particularly, the first peak is larger than 4.2 pN and the second peak is smaller than 8.4 pN. These results suggest that the transient binding and unbinding of kinesins and the nonuniform distribution of forces among the engaged kinesins has a smoothing effect on the probability distribution of the stall force. The stall force is likely to have values between the stall forces of a single kinesin and two kinesins. In addition, a stall force larger than 8.4 pN is frequently observed, as shown in Fig. 4(c).

Next, the cargo is placed near a 90° intersection of two MTs, and the transport direction and time are calculated. Similarly to the experimental setup [18], the bottom MT is attached to a glass slide by proteins with an approximate length of 135 nm [Fig. 4(d)]. In the underpass situation, at the beginning, the cargo is placed at a random place 1 μm away from the surface of MT2 and 400 nm away from the surface of MT1. No kinesin binds to the MTs. At every time step, the cargo diffuses and the binding probabilities of all kinesins are calculated. When at least one kinesin binds to MT1, the cargo is transported toward the MT intersection. The simulation finishes when the cargo moves 1 μm away from the intersection or the simulation time exceeds 8 s. In the overpass situation, the cargo is placed at a random place 1 μm from the surface of MT1 and 400 nm from the surface of MT2. The cargo motions are classified into four different types based on the following criteria. If the cargo moves 1 μm away from the intersection on the original MT in 3 s, then the motion is defined as passing. If the cargo switches to the intersecting MT, and moves 1 μm away from the intersection in 3 s, the motion is defined as switching. If the cargo remains at the intersection longer than 3 s, then the motion is defined as pausing. If the cargo diffuses away from two MTs and does not rebind in 3 s, the motion is defined as dissociation. To verify the model, the probability distribution of the four types of cargo motions is calculated when $N = 36$ and compared with experiments [18]. Note that, to calibrate the variation in probabilities influenced by the number of simulations, 1000 simulations are performed. The results are devided into 10 groups to acquire the error bars shown in Figs. 4(e) and 4(f). In the underpass situation, the top MT impedes the cargo from moving forward on the original MT and increases the switching probability [Fig. 4(e)]. In the overpass situation, the cargo can be transported above the two MTs and can pass the intersection. Overall, the modeling results show good agreement to the experiments [18]. In addition, the dwell time that a cargo spends at the MT intersection is calibrated (Fig. 6). In the underpass situation, the mean dwell time at the intersection is 4.7 s. In the overpass situation, the mean dwell time at the intersection is 4.8 s. If the cargo is transported along the MT between two intersections, then the time for the cargo to move 2 μm is around 3.3 s (assuming the velocity is 600 nm/s). Thus, the intersection slows down the transport.

B. Transport dynamics influenced by MT topology

Based on the model, the effects of the topology of a MT intersection on the transport dynamics are studied. As shown in Figs. 7(a) and 7(d), the intersection topology can be characterized by the distance H and angle β. H is defined as the shortest distance between the surfaces of two MTs. The intersection distance H is varied from 0 nm to 1000 nm. When $H > 1000$ nm, the intersected MT has negligible effects on the transport. β is defined as the angle between the two MTs. β varies between 0° and 180°. The number of kinesins on the cargo is 36.

In the overpass situation [Figs. 7(b) and 7(e)], the cargo motion is less influenced by the bottom MT. Cargo is likely to move above the two MTs, and the kinesins is not long enough to bind to the bottom MT. Therefore, the probability of passing is large and less influenced by the intersection topology.

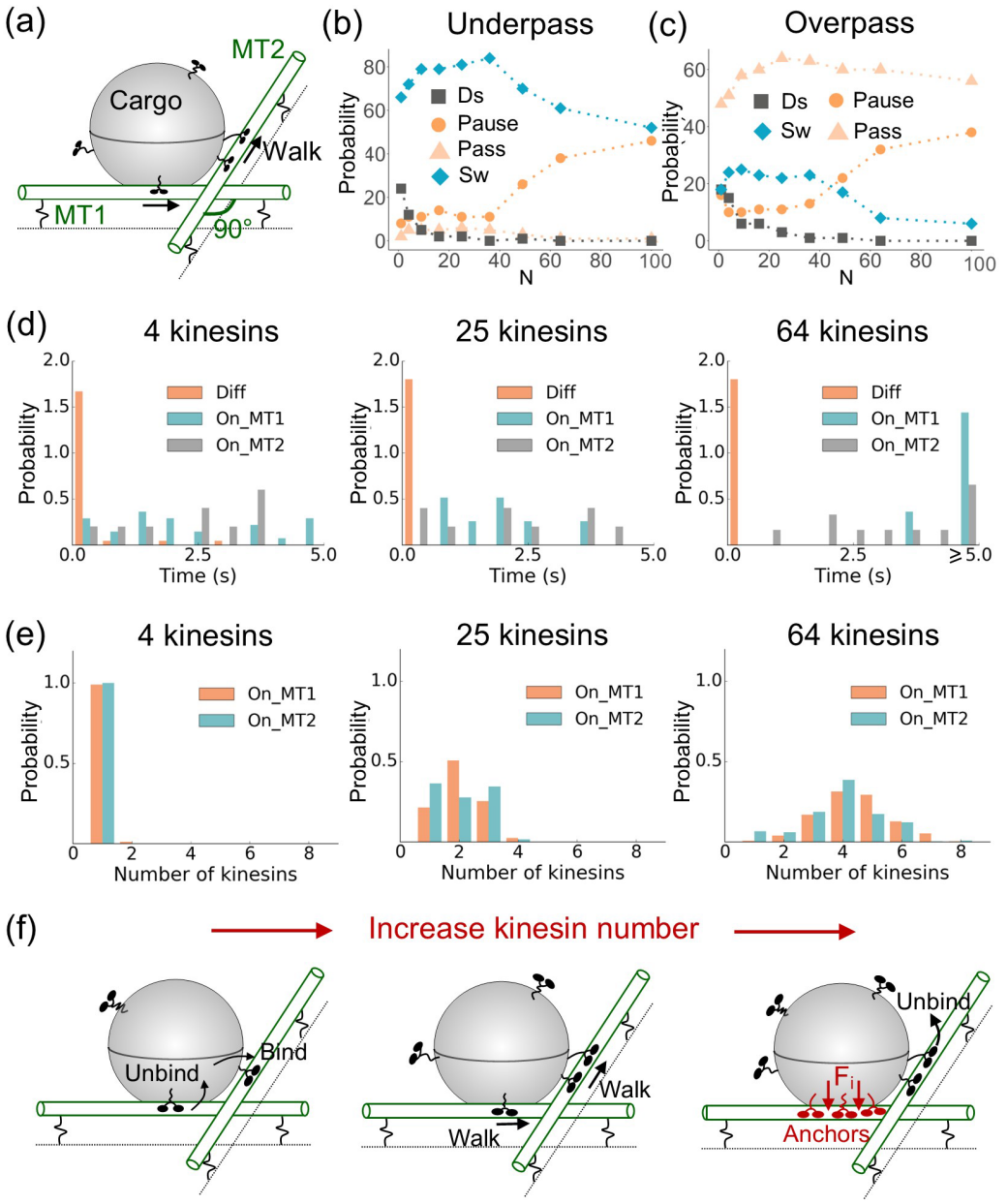

FIG. 9. The collective transport dynamics influenced by the number of kinesins N at a 90° MT intersection. (a) The schematic view of a cargo being transported along the bottom MT and switching to the top MT at the intersection. The intersection distance is 0 nm. [(b) and (c)] The influence of the number of kinesins N on the transport dynamics when the cargo is transported along the bottom MT (b) or the top MT (c) toward the intersection. (d) In the underpass situation, the distribution of the association time on MT1 and MT2 as well as the diffusion time when N is 4, 25, and 64. (e) In the underpass situations, the distribution of the number of associated kinesins on MT1 and MT2 over different N. (f) The schematic illustration of the influence of kinesin number N on the transport dynamics.

In the underpass situation [Figs. 7(c) and 7(f)], the transport of a cargo by multiple kinesins are less influenced by the intersection distance H compared to the transport by a single kinesin. However, a decrease in the switching probability is still noticeable as H increases. When $H \leqslant 200$ nm, the decrease is caused by the geometrical barrier of the intersection. Cargo rotates at the intersection due to the moment generated by kinesins. When $H \geqslant 800$ nm, the switching probability decreases because cargo can pass the intersection through the gap between the two MTs. The model also predicts that the switching probability is maximized when the two MTs are perpendicularly attached. When $\beta = 90^\circ$, the average number of kinesins on MT2 and the time duration when at least one kinesin binds to MT2 are the largest (Fig. 8). Therefore, the switching probability is enhanced because more kinesins pull the cargo along the intersecting MT for a longer time. When $\beta > 90^\circ$, the antagonistic dynamics between kinesins on two MTs accelerates their unbinding probabilities. Note that, when the intersection distance $H > 0$ nm, the influence of the intersection angle β on transport dynamics can be different. For example, Bergman *et al.* [37] showed that the switching probability is the largest when $\beta = 90^\circ$ and $H = 0$ nm. However, when H is equal to the cargo radius or diameter, the switching probability is small at the 90° intersection. In

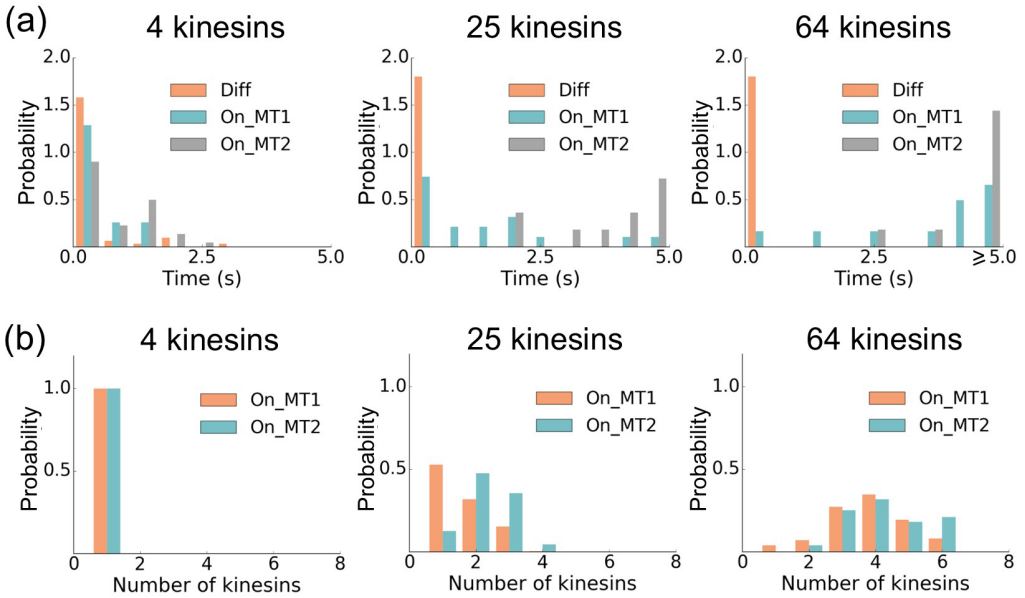

FIG. 10. The collective transport dynamics influenced by the number of kinesins N in the overpass situation. (a) The distribution of the association time on MT1 and MT2 as well as the diffusion time when N is 4, 25, and 64. (b) The distribution of the number of associated kinesins on MT1 and MT2 over different N. The intersection distance is 0 nm and the intersection angle is 90°.

addition, the latest work from Higuchi *et al.* [56,57] observed frequent direction changes in very acute or obtuse angles inside MT networks in living cells. Thus, these results indicate that the distances between intersected MTs *in vivo* are likely to be larger than 0 nm and comparable to the radius of intracellular cargoes. Bálint *et al.* [58] measured the intersection distances inside monkey kidney cells and showed that the intersection distances vary from 100 to 600 nm. Therefore, our model predictions are consistent with previous findings.

C. Transport dynamics influenced by the number of kinesins

To understand the effects of the number kinesins (usually quantified by the kinesin concentration in experiments) on the intracellular cargo transport in different MT topologies, multiple analyses are performed. First, when the cargo is transported toward a 90° intersection of two MTs, the probabilities of an 800 nm-cargo passing, pausing, switching and dissociating at the intersection are calculated over different number of kinesins N. In the underpass situation, when $N <$ 16, only one kinesin is likely to bind to the MTs [Fig. 9(e)]. Thus, the cargo dissociation probability is large. When $N \in$ [16,35], the cargo has the largest switching probability, because some kinesins bind to MT1 to prevent cargo dissociation and more kinesins start to bind to MT2 to switch transport direction. A longer average association time on MT2 than on MT1 ensures cargo moving away from the intersection [Fig. 9(d)]. When $N > 36$, the number of kinesins that bind to the original track increases considerably. When $N = 64$, the average number of kinesins bind to MT1 is around 4.4. Since unbinding 4 kinesins simultaneously requires a large force, the cargo is likely to be trapped near MT1. Similarly, in the overpass situation, when an intermediate number of kinesins are attached to the cargo ($N = 25$), multiple kinesins bind to MT2 for a sufficient long time, which leads to the large passing probability (Fig. 10). Note that, the proportion distribution of kinesins on different MTs at the intersection depends on the cargo levitation and the external torque (Fig. 11). For example, when the cargo is levitated above, a larger proportion of kinesins are going to bind to MT2 because of the limited length of the cargo linkers. When a counter clockwise torque is applied to the cargo, the forces between kinesins and MT1 increase, which accelerates the unbinding from MT1 and modifies the proportion distribution of kinesins.

Next, the transport dynamics on a bundle of two parallel MTs is studied. The distance between the surfaces of the two parallel MTs is set to be 15 nm in this study. Compared to a single MT, a parallel bundle has more binding sites reachable to kinesins. Thus, when $N \geqslant 36$, the average number of kinesins on the bundle is larger than on a single MT (Fig. 5). In the simulation, the cargo position $\boldsymbol{X}_{\mathrm{cg}}$ over time t is recorded.

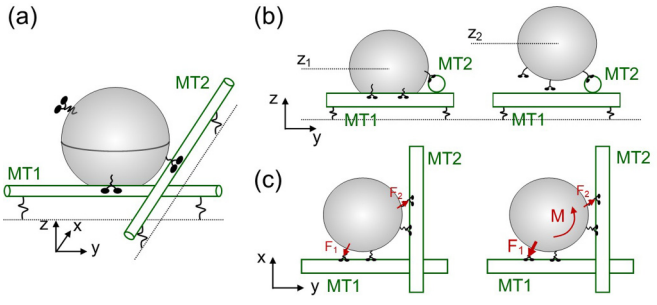

FIG. 11. Schematic illustration of the influence of cargo levitation and torque diffusion on the proportion distribution of motors on different MTs. (a) Kinesins transport the cargo from MT1 toward the intersection. (b) Cargo levitation increases the proportion of kinesins on MT2 by changing the distances between the cargo and MTs. (c) A counterclockwise torque changes forces inside the kinesins and increases the proportion of kinesins on MT2.

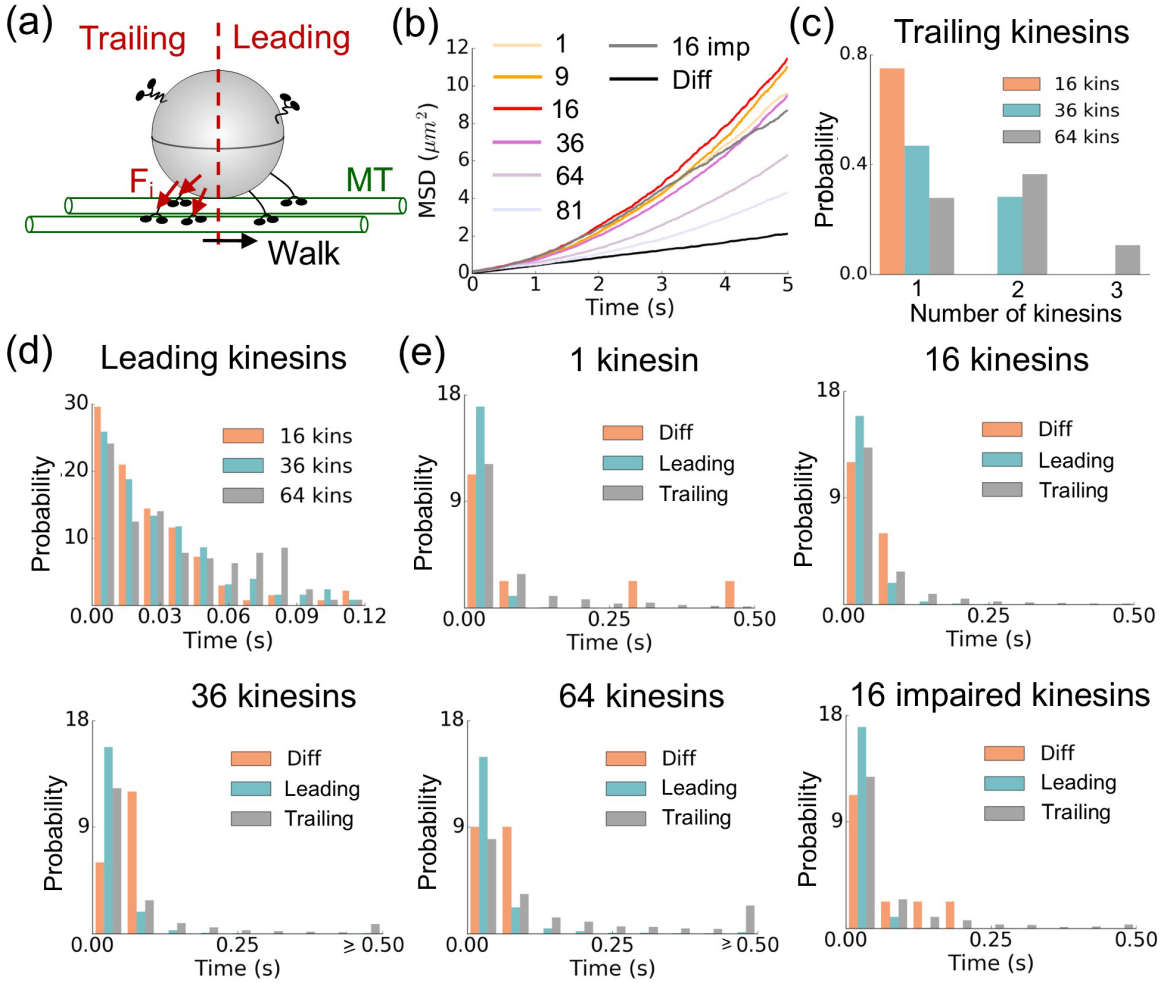

FIG. 12. The collective transport dynamics influenced by kinesin number N along a parallel MT bundle. (a) The schematic illustration of the kinesins binding between the cargo and the MTs. Kinesins are classified as trailing kinesins and leading kinesins based on whether the positions of their heads locate behind the center of the cargo. (b) The MSDs of the cargo over different number of kinesins N. The motion of the cargo is superdiffusive because of the active forces applied by kinesins. In addition, the gray line represents the MSD of the cargo transported by 16 impaired kinesins. The impairment of the kinesin is defined as decreasing the binding rate k_{b0} to half of its original value and increasing the unbinding rate P_{u0} and k_{u0} to twice of the original values. (c) The distribution of the number of trailing kinesins when N is 16, 36, and 64. (d) The distribution of the duration of a chemical reaction cycle for the leading kinesins over N. (e) The distribution of the association time of the trailing and leading kinesins on the MTs and the diffusion time over N.

Then, the mean-square displacement (MSD) of the cargo, calculated as $\mathrm{MSD}(t) = \frac{1}{100}\sum_{i=0}^{100}[\boldsymbol{X}_{cgi}(t) - \boldsymbol{X}_{cgi}(t=0)]^2$ is used to represent the cargo motility. $\boldsymbol{X}_{cgi}$ is the position of the cargo at time t in ith simulation. We found that the average MSD is the largest when $N = 16$ [Fig. 12(b)]. When $N = 1$, the variation of the MSD curves is large (Fig. 13) because the only one kinesin connecting between the cargo and the bundle is likely to unbind and the transport is disrupted accordingly. Increasing the kinesin number N reduces the variation (Fig. 13), which suggests the transport becomes more robust. However, when $N \geqslant 36$, the slopes of all MSD curves are low, indicating transport becomes slower. In addition, when the cargo is transported by impaired kinesins which have a larger unbinding probability (i.e., twice of its original value) and smaller binding probability (i.e., half of its original values), the 100 realizations of MSDs become close to the situation when $N = 1$ (Fig. 13). To understand the mechanism that leads to the decreasing of the transport velocity when N is large, the distribution of the duration of a chemical cycle of leading kinesins, the number of trailing kinesins, and the association time of the trailing and leading kinesins are calculated. Note that, a trailing kinesin is defined as a kinesin whose heads attach to the binding sites behind the center of the cargo along the MT direction. A leading kinesin has heads attaching to positions ahead of the cargo center [Fig. 12(a)]. Trailing kinesins pull the cargo back and apply resisting force on the leading kinesins. The resisting force slows down the stepping frequency of the leading kinesins [see video in the Supplemental Material at [46] and Fig. 14(b)]. On the MT bundle, as N increases, more kinesins bind behind the cargo center [Fig. 12(c)]. A large number of trailing kinesins causes the long duration of a chemical reaction on the leading kinesin heads [Fig. 12(d)]. At the same time, a large N reduces the diffusion time and increases the association time on both MTs. However, the increasing of the association time for the trailing motors is faster than the

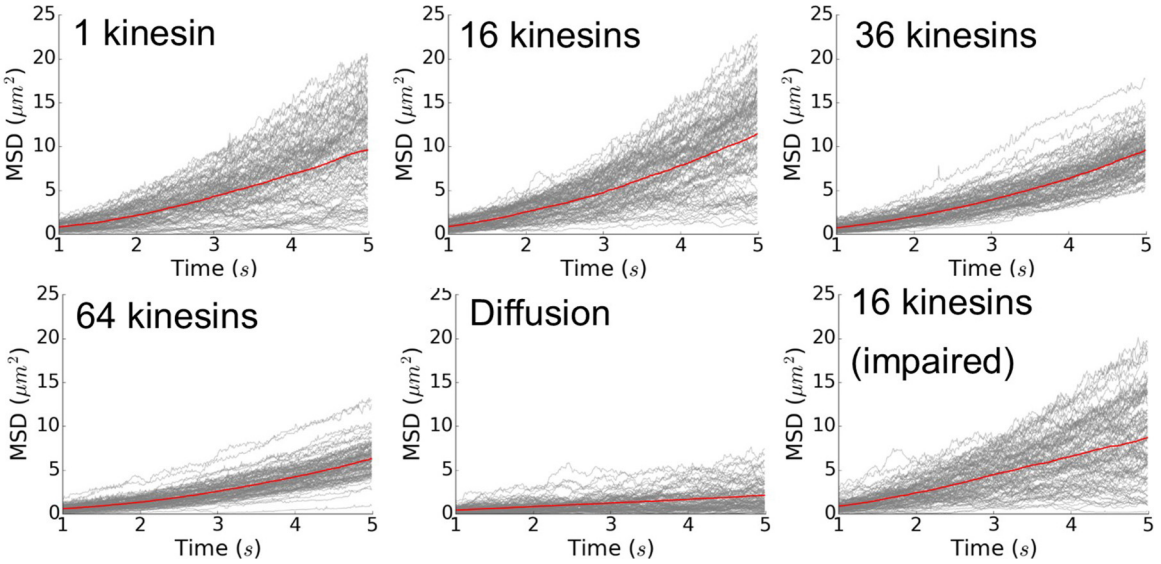

FIG. 13. The realization of 100 simulation results of the MSDs along a parallel MT bundle over different kinesin number N. The gray lines are the MSDs over time calculated in each of the 100 simulations. Red lines are the ensemble average of the 100 MSD curves.

leading motors. When $N \geqslant 36$, some trailing motors remain binding to the MT for more than 5 s. Thus, the transport speed and cargo mobility are reduced at the high kinesin concentration.

The interference of a neighboring MT on the transport is considered in order to study the robustness of the transport along a MT bundle for different numbers of kinesins. In the model, the neighboring MT is placed perpendicularly to the bundle consisting of two parallel MTs, and the distance between the surfaces of the intersecting MT and the bundle is chosen to be 850 nm so cargo can move through the gap between the two parallel MTs and the neighboring MT, as shown in Fig. 15(a). Initially, the cargo is transported on the MT bundle toward the neighboring MT. When the cargo fails to move 1 μm away from the neighboring track in 3 s, or when the cargo switches moving direction, or when it dissociates from the MT, the transport is defined as disrupted. Based on the model, the probability of passing the neighboring MT without being disrupted is calculated over the number of kinesins N [Fig. 15(b)]. When $N = 16$, the largest passing probability is achieved. When $N > 16$, some kinesins are expected to bind to the intersecting MT and disturb the transport. When $N \leqslant 9$, the interference between the cargo and the intersecting MT increases the dissociation probability.

IV. CONCLUSION

This paper proposed a 3D stochastic multiphysics model to study the collective cargo transport by multiple kinesins in different topologies of MTs. Based on the model, three important biological insights are observed.

First, when two identical kinesins pull a common cargo together along a track, the external load applied on the cargo is not equally distributed among all kinesins such that the contribution of each kinesin to the cargo transport is different. When two kinesins are attached to adjacent positions on the surface of the cargo, the forces inside the two kinesins are small and almost symmetrically distributed about 0 pN. The distribution of the predicted time duration of a chemical reaction cycle is shown in Fig. 14(a). The estimated average time duration calculated is 0.015 s. Since kinesin moves 8 nm in each step, the average velocity of the two kinesins is around 533 nm/s. The predicted average time duration of the two kinesins is similar to the experimentally measured value of a single kinesin walks along a MT [42,59]. Thus, the two kinesins transport the cargo independently. When the two kinesins are attached to distant positions on the surface of the cargo, the average forces in the two kinesins increase. The trailing kinesin experiences an assisting force while the leading kinesin experiences a resisting force [Fig. 14(b)]. Under an external load opposite to the transport direction, cargo diffuses back. The leading kinesin extends longer than the trailing kinesin and shares a larger force. Therefore, the time duration of the chemical reaction on the leading kinesin heads is significantly increased [Fig. 14(c)]. The leading kinesin is likely to be stalled and the trailing kinesin keeps walking. Our analysis provides a plausible explanation to the experiments, in which Jamison *et al.* [16] measured the force velocity curve of two kinesins separated by a DNA-based molecular scaffold with fixed length. They found that the measured force velocity curve of two kinesins is different from the theoretically generated curve assuming each motor shares half of the applied load and two motors do not interact. Specifically, the measured walking velocity of two kinesins is slower than the theoretically predicted values at low loads because of the antagonistic dynamics, and the velocity is faster at large loads because of the synergistic dynamics. Interestingly, Uar *et al.* showed [60] that two identical dyneins tend to share load equally in both steady state and during the initial building up of internal elastic strains. It is likely the properties of two motors, such as the length, stiffness, binding rate and unbinding rate, play important roles in motor cooperativity. For example, Uar *et al.* [61] observed that the average force generated by several strong motors with larger stall force and large unbinding rate, such as kinesin-1, deviate strongly from their collective stall force. It suggests that

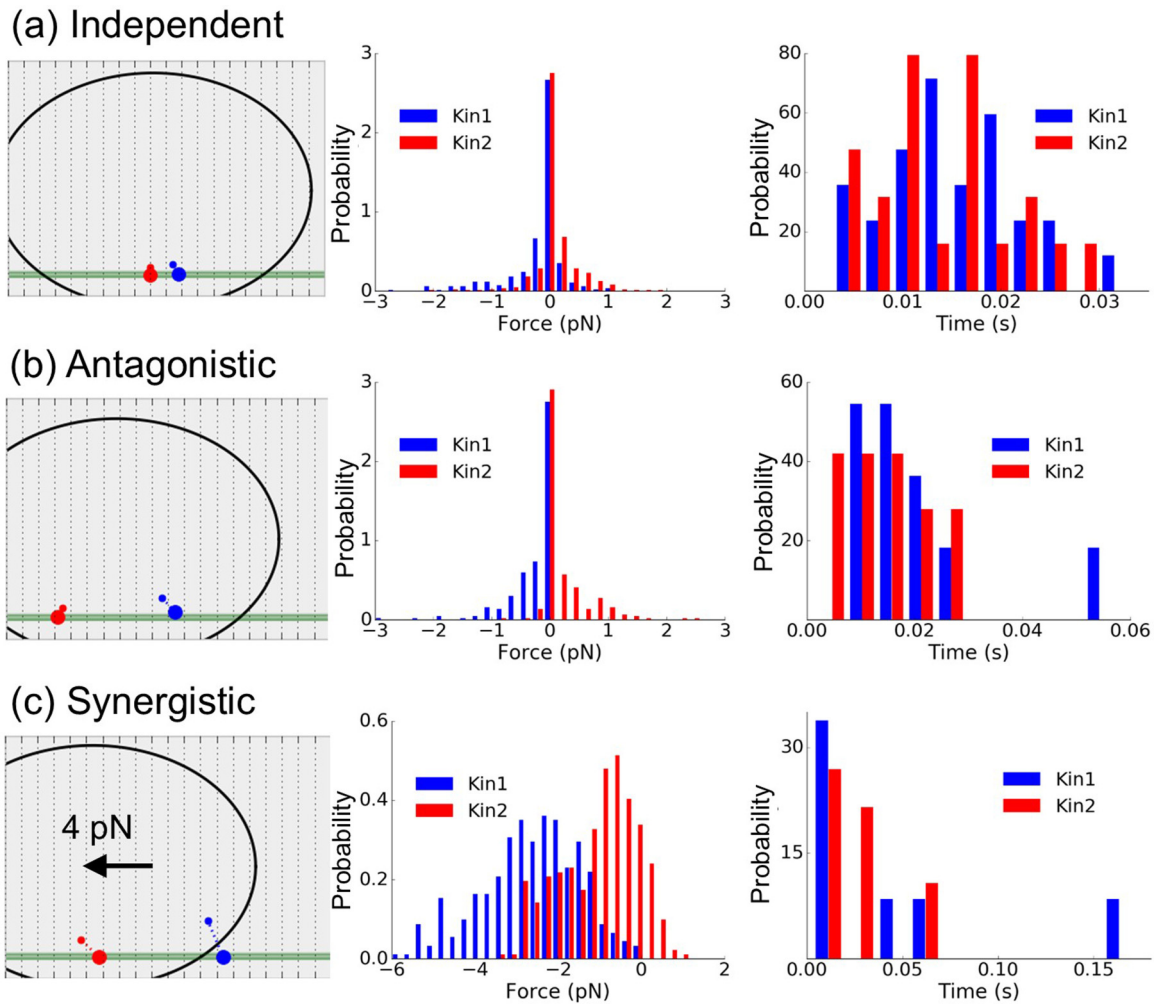

FIG. 14. Three types of collective kinesin dynamics (of two kinesins) along a single MT. (a) Independent dynamics happens when two identical kinesins walk with similar stepping rate and pull the cargo. (b) Antagonistic dynamics is caused by the two kinesins pull the cargo toward different directions. The leading kinesin experiences a resisting force and the chemical reaction on its heads is likely to be slowed down. (c) Synergistic dynamics helps two kinesins transport the cargo under an external load. The leading kinesin shares a larger load and its chemical reaction happens slower than the trailing kinesins. The first column of the plots contains the schematic representations of the cargo (black circle), MT (green line), and two kinesins. The leading kinesin (kinesin 1) is represented as blue. The trailing kinesin (kinesin 2) is represented as red. The second column of plots represent the distribution of forces inside the two kinesins. Positive values represent the direction of the force is the same as the walking direction. The third column of plots are the distributions of the time a kinesin takes to complete a chemical reaction cycle and walk one step forward.

strong motors tend to have a worse cooperativity, probability because motors detach from the track during strain generation. Wang *et al.* [62] showed that the degree of cooperativity of two kinesin motors is influenced by the stiffness of the cargo linker, unbinding rate, and stepping rate. In particular, a smaller unbinding rate, a lower cargo linker stiffness and a larger stepping rate lead to a higher motor cooperativity and a longer run length. Arpağ *et al.* [32] found that the cotransport by slow kinesin-1 and fast kinesin-3 is likely to be dominated by kinesin-1, because the leading kinesin-3 can rapidly unbind and re-equilibrate their positions near the cargo, whereas the trailing kinesin-1 continue to pull. In our study, it is shown that the influence of the cotransport is originated from the different extensions of the kinesin cargo linkers. Therefore, when the length of the cargo linker of the leading kinesin is longer than the trailing kinesin, the transport is expected to be more robust to external loads. To confirm this behavior, additional experiments on the run lengths and velocities of the cargo mediated by motors with different lengths are needed. Second, trailing kinesins could impair the cargo transport. Ross *et al.* [18] measured the probabilities of passing, switching, pausing and dissociation at the 90° MT intersection over different kinesin concentrations. They found that the pausing probability increases, and the switching probability decreases at high kinesin concentration. Based on the model, we show that the changes in the switching and pausing probabilities over kinesin concentrations are caused by the fact that several trailing kinesins bind to the original MT and act as anchors to prevent cargo being transported away from the intersection. When multiple kinesins walk on the parallel MT bundle toward the same direction, we found that the cargo mobility is reduced when too many kinesins are involved. This

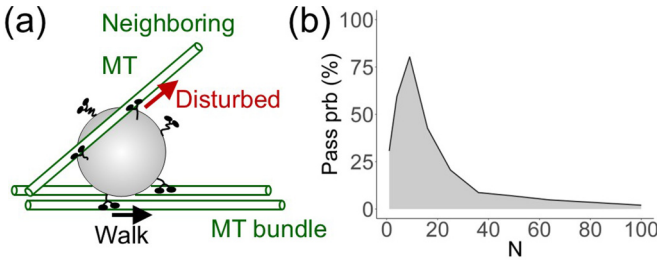

FIG. 15. The interruption of a neighboring MT on the transport for various number of kinesins N. (a) An illustration of the situation when a cargo is transported by kinesins along two parallel MTs. Extra kinsesins on the cargo can bind to the neighboring track and disrupt the transport. The neighboring track is placed perpendicularly to the two parallel MTs. The shortest distance between the surfaces of the neighboring MT and the two parallel MTs is 850 nm. (b) The probability of passing the neighboring MT without being disrupted over different value of N.

phenomenon is reminiscent to the negative correlation between the transport velocity and motor concentration observed in previous experiments [22,25,63]. Specifically, Shubeita *et al.* [22] found that the average transport velocity of the lipid droplets in the embryos with reduced kinesin concentration was approximately 5.5% higher than in wild-type embryos. Telley *et al.* [63] measured the concentration dependence of motor characteristics, including the run length, dwell time, velocity and binding rate. The slow transport at high motor concentration is usually explained as the binding sites on the MT being fully occupied by the abundant motors such that the unbinding rates of kinesins is increased and binding rates are decreased. In this work, we have shown that the excessive trailing motors could also reduce the transport via the mechanical interactions between motors. In general, the pausing phenomenon during the transport generated by excessive trailing motors could be one of the major causes of the subdiffusive cargo motor inside the cells [64,65]. Zaburdaev *et al.* [66] mathematically showed that by varying the power law tails of the distribution of the pausing time, all the diffusion regimes (i.e., normal diffusion, superdiffusion, and subdiffusion) can be accessed. However, whether and at what motor concentration the active transport will be overwhelmed by the increased pausing time in different topology of MTs needs to be studied further. Third, the microscopic dynamics of kinesins depends on geometrical information, including the distribution of kinesins on the cargo, the relative position of the cargo on the MTs, and the topology of MTs. Therefore, changing the geometrical information will lead to changes in the microscopic kinesin dynamics. However, as an average outcome of these microscopic dynamics, the macroscopic properties of the transport (i.e., the ability to persist in the transport direction and move fast) show surprising similarities in different MT topologies. Specifically, we predict that there is an optimal number of kinesins to transport a cargo pass MT intersections and along MT bundles.

The 3D stochastic dynamic model proposed here can be extended to characterize more complex and *in vivo*–like situations. For example, the low stiffness of the intracellular cargoes can influence the collective dynamics of kinesins. Due to the compliance of the soft cargo, more kinesins can bind to the MT, but the mechanical coupling among kinesins becomes weaker. *In vitro* methods, including the DNA scaffolds and modifying the anchor point of motors on the cargo surface [12,67] have been used to study different mechanical couplings of kinesin motors. Combining our model with these *in vitro* experiments, general transport dynamics influenced by the coupling stiffness and the distance between kinesins can be investigated. Moreover, it would be also interesting to study whether the selective transport of different types of intracellular cargoes to their own destinations is determined by the cargo stiffness, and whether the failure of intracellular transport under disease conditions is influenced by changes in cargo stiffness.

[1] J.-W. Tsai, W.-N. Lian, S. Kemal, A. R. Kriegstein, and R. B. Vallee, Nat. Neurosci. **13**, 1463 (2010).
[2] T. Sanchez, D. Welch, D. Nicastro, and Z. Dogic, Science **333**, 456 (2011).
[3] K. Svoboda, C. F. Schmidt, B. J. Schnapp, and S. M. Block, Nature **365**, 721 (1993).
[4] S. M. Block, L. S. B. Goldstein, and B. J. Schnapp, Nature **348**, 348 (1990).
[5] A. Yildiz, M. Tomishige, R. D. Vale, and P. R. Selvin, Science **303**, 676 (2004).
[6] P. D. Chowdary, D. L. Che, L. Kaplan, O. Chen, K. Pu, M. Bawendi, and B. Cui, Sci. Rep. **5**, 18059 (2015).
[7] D. Ando, M. K. Mattson, J. Xu, and A. Gopinathan, Sci. Rep. **4**, 7255 (2014).
[8] C. L. Asbury, A. N. Fehr, and S. M. Block, Science **302**, 2130 (2003).
[9] N. J. Carter and R. A. Cross, Nature **435**, 308 (2005).
[10] M. Vershinin, B. C. Carter, D. S. Razafsky, S. J. King, and S. P. Gross, Proc. Natl. Acad. Sci. USA **104**, 87 (2007).
[11] C. Leduc, F. Ruhnow, J. Howard, and S. Diez, Proc. Natl. Acad. Sci. USA **104**, 10847 (2007).
[12] K. Furuta, A. Furuta, Y. Y. Toyoshima, M. Amino, K. Oiwa, and H. Kojima, Proc. Natl. Acad. Sci. USA **110**, 501 (2013).
[13] J. Beeg, S. Klumpp, R. Dimova, R. S. Gracià, E. Unger, and R. Lipowsky, Biophys. J. **94**, 532 (2008).
[14] S. Bhaban, D. Materassi, M. Li, T. Hays, and M. Salapaka, PLoS Comput. Biol. **12**, e1005152 (2016).
[15] S. Klumpp and R. Lipowsky, Proc. Natl. Acad. Sci. USA **102**, 17284 (2005).
[16] D. K. Jamison, J. W. Driver, A. R. Rogers, P. E. Constantinou, and M. R. Diehl, Biophys. J. **99**, 2967 (2010).
[17] H. W. Schroeder, C. Mitchell, H. Shuman, E. L. Holzbaur, and Y. E. Goldman, Curr. Biol. **20**, 687 (2010).
[18] J. L. Ross, H. Shuman, E. L. Holzbaur, and Y. E. Goldman, Biophys. J. **94**, 3115 (2008).
[19] Y. Gao, S. M. Anthony, Y. Yu, Y. Yi, and Y. Yu, Biophys. J. **114**, 2900 (2018).
[20] L. Stepanek and G. Pigino, Science **352**, 721 (2016).

[21] I. Neri, N. Kern, and A. Parmeggiani, Phys. Rev. Lett. **110**, 098102 (2013).

[22] G. T. Shubeita, S. L. Tran, J. Xu, M. Vershinin, S. Cermelli, S. L. Cotton, M. A. Welte, and S. P. Gross, Cell **135**, 1098 (2008).

[23] C. Leduc, K. Padberg-Gehle, V. Varga, D. Helbing, S. Diez, and J. Howard, Proc. Natl. Acad. Sci. USA **109**, 6100 (2012).

[24] L. Reese, A. Melbinger, and E. Frey, Biophys. J. **101**, 2190 (2011).

[25] D. M. Miedema, V. S. Kushwaha, D. V. Denisov, S. Acar, B. Nienhuis, E. J. G. Peterman, and P. Schall, Phys. Rev. X **7**, 041037 (2017).

[26] R. Lipowsky, S. Klumpp, and T. M. Nieuwenhuizen, Phys. Rev. Lett. **87**, 108101 (2001).

[27] P. C. Bressloff and J. M. Newby, Rev. Mod. Phys. **85**, 135 (2013).

[28] J. Xu, S. J. King, M. Lapierre-Landry, and B. Nemec, Biophys. J. **105**, L23 (2013).

[29] M. Rank and E. Frey, Biophys. J. **115**, 1068 (2018).

[30] S. M. Block, C. L. Asbury, J. W. Shaevitz, and M. J. Lang, Proc. Natl. Acad. Sci. USA **100**, 2351 (2003).

[31] S. M. B. Koen Visscher, and Mark J. Schnitzer, Nature **400**, 184 (1999).

[32] G. Arpağ, S. R. Norris, S. I. Mousavi, V. Soppina, K. J. Verhey, W. O. Hancock, and E. Tüzel, Biophys. J. **116**, 1115 (2019).

[33] K. Uppulury, A. K. Efremov, J. W. Driver, D. K. Jamison, M. R. Diehl, and A. B. Kolomeisky, J. Phys. Chem. B **116**, 8846 (2012).

[34] H. Khataee and J. Howard, Phys. Rev. Lett. **122**, 188101 (2019).

[35] G. I. Bell, Science **200**, 618 (1978).

[36] R. Blackwell, D. Jung, M. Bukenberger, and A.-S. Smith, Sci. Rep. **9**, 18373 (2019).

[37] J. P. Bergman, M. J. Bovyn, F. F. Doval, A. Sharma, M. V. Gudheti, S. P. Gross, J. F. Allard, and M. D. Vershinin, Proc. Natl. Acad. Sci. USA **115**, 537 (2018).

[38] Q. Wang, M. R. Diehl, B. Jana, M. S. Cheung, A. B. Kolomeisky, and J. N. Onuchic, Proc. Natl. Acad. Sci. USA **114**, E8611 (2017).

[39] S. P. Gilbert, M. L. Moyer, and K. A. Johnson, Biochemistry **37**, 792 (1998).

[40] D. D. Hackney, Proc. Natl. Acad. Sci. USA **102**, 18338 (2005).

[41] A. G. Hendricks, B. I. Epureanu, and E. Meyhöfer, Nonlinear Dyn. **53**, 303 (2008).

[42] M. Schnitzer, K. Visscher, and S. Block, Nat. Cell Biol. **2**, 718 (2000).

[43] J. Andreasson, B. Milic, G.-Y. Chen, N. Guydosh, W. Hancock, and S. Block, Elife **4**, e07403 (2015).

[44] R. P. Erickson, Z. Jia, S. P. Gross, and C. C. Yu, PLoS Comput. Biol. **7**, e1002032 (2011).

[45] W. Nam and B. I. Epureanu, PLoS ONE **11**(1) (2016).

[46] See Supplemental Material at http://link.aps.org/supplemental/10.1103/PhysRevE.101.052413 for stepping probabilities and values of ADK and ABK used in the simulation.

[47] S. Jeney, E. H. K. Stelzer, H. Grubmüller, and E.-L. Florin, ChemPhysChem **5**, 1150 (2004).

[48] J. Kerssemakers, J. Howard, H. Hess, and S. Diez, Proc. Natl. Acad. Sci. USA **103**, 15812 (2006).

[49] K. Chen, W. Nam, and B. I. Epureanu, Phys. Rev. E **98**, 052412 (2018).

[50] W. Nam and B. I. Epureanu, PLoS Comput. Biol. **11**, 1 (2015).

[51] K. Kawaguchi, S. Uemura, and S. Ishiwata, Biophys. J. **84**, 1103 (2003).

[52] F. Berger, S. Klumpp, and R. Lipowsky, Nano Lett. **19**, 2598 (2019).

[53] L. Romberg and R. D. Vale, Nature **361**, 168 (1993).

[54] A. Yildiz, M. Tomishige, A. Gennerich, and R. D. Vale, Cell **134**, 1030 (2008).

[55] K. H. Kuniyoshi Kaseda and H. Higuchi, Nat. Cell Biol. **5**, 1079 (2003).

[56] S. Lee and H. Higuchi, Biomed. Opt. Express **10**, 6611 (2019).

[57] S. Lee, H. Kim, and H. Higuchi, Opt. Express **26**, 16236 (2018).

[58] Š. Bálint, I. Verdeny Vilanova, Á. Sandoval Álvarez, and M. Lakadamyali, Proc. Natl. Acad. Sci. USA **110**, 3375 (2013).

[59] M. L. Moyer, S. P. Gilbert, and K. A. Johnson, Biochemistry **37**, 800 (1998).

[60] M. C. Uçar and R. Lipowsky, Sci. Rep. **9**, 454 (2019).

[61] M. C. Uar and R. Lipowsky, Nano Lett. **20**, 669 (2020).

[62] Q. Wang and A. B. Kolomeisky, J. Phys. Chem. B **123**, 5805 (2019).

[63] I. A. Telley, P. Bieling, and T. Surrey, Biophys. J. **96**, 3341 (2009).

[64] S. M. A. Tabei, S. Burov, H. Y. Kim, A. Kuznetsov, T. Huynh, J. Jureller, L. H. Philipson, A. R. Dinner, and N. F. Scherer, Proc. Natl. Acad. Sci. USA **110**, 4911 (2013).

[65] M. Otten, A. Nandi, D. Arcizet, M. Gorelashvili, B. Lindner, and D. Heinrich, Biophys. J. **102**, 758 (2012).

[66] V. Zaburdaev, S. Denisov, and J. Klafter, Rev. Mod. Phys. **87**, 483 (2015).

[67] A. Rai, D. Pathak, S. Thakur, S. Singh, A. K. Dubey, and R. Mallik, Cell **164**, 722 (2016).